

# Krylov Subspace Method for Molecular Dynamics Simulation based on Large-Scale Electronic Structure Theory

Ryu Takayama<sup>1,2</sup>, Takeo Hoshi<sup>2</sup> and Takeo Fujiwara<sup>2</sup>

<sup>1</sup> Research and Development for Applying Advanced Computational Science and Technology,  
Japan Science and Technology Agency, 4-1-8 Honcho, Kawaguchi-shi, Saitama 332-0012, Japan

<sup>2</sup> Department of Applied Physics, University of Tokyo, 7-3-1 Hongo, Bunkyo-ku, Tokyo 113-8656, Japan

For large scale electronic structure calculation, the Krylov subspace method is introduced to calculate the one-body density matrix. Its arithmetic structure is studied for its validation. Molecular dynamics simulation of Si(001) surface reconstruction is examined as an example, and the results reproduce the essential mechanism of asymmetric surface dimer. An appropriate choice of controlling parameters is discussed for the efficient and practical calculation.

**KEYWORDS:** Krylov subspace, large scale electronic structure calculations, density matrix, tight-binding molecular dynamics, surface reconstruction, parallel computation, hybrid scheme within quantum mechanics

## 1. Introduction

The study of nanoscale systems requires a large-scale atomistic simulations with quantum mechanical freedoms of electrons. The practical requirement to carry out the simulations is how to extract desired quantities from a given large Hamiltonian matrix, not only accurately but also efficiently. Simulation methods in large scale systems have been studied already in the last decade.<sup>1,3</sup> In order to execute molecular dynamics simulation, one needs information about the total energy and forces on an individual atom, and these physical quantities should be obtained by means of either eigen states  $\psi_i$  or the one-body density matrix of the system;

$$\langle X^i \rangle = \sum_j \langle \psi_j | \hat{X} | \psi_j \rangle \frac{f_j}{k_B T} \quad (1)$$

Here  $f_j = \frac{1}{k_B T}$  is the Fermi-Dirac distribution function.

The molecular dynamics calculation in large-scale systems can be done on the basis of transferable short-range tight-binding Hamiltonians  $H$ , where we calculate the physical property  $\langle X^i \rangle$  as

$$\langle X^i \rangle = \text{Tr}[\hat{X}] = \sum_{ij} X_{ji} \quad (2)$$

Here  $i$  and  $j$  are sites of atomic site and orbital. The energy and forces acting on an atom are contributed only by elements that have non-zero values of the Hamiltonian matrix. In other words, even though the density matrix is of long range, only the short range behavior of the density matrix is essential.<sup>4</sup> Therefore, the essential methodology for large scale calculations is how to obtain the short range part of the density matrix without calculating eigen states of the original Hamiltonian. The essential point here is the fact that we adopt the short-range tight-binding Hamiltonian and this makes computation local. We will only comment here that the short-range tight-binding Hamiltonian can be always constructed both in

insulators and metals from the first principle theory.<sup>5</sup>

We have developed a set of methods, without calculating eigenstates, of large-scale atomistic simulations, which are based on generalized Wannier state and hybrid scheme within fully quantum mechanical description of electron systems.<sup>6,10</sup> These methods are rigorously a linear scale simulation in atom number, and were tested upto  $10^6$  atoms by using a standard workstation. The generalized Wannier states are defined formally as unitary transformation of the occupied eigen states, though eigen states are not actually obtained. This method is practical and efficient in covalent bonded materials, where the localized Wannier states reproduce well the electronic structure energy and the density matrix, at least its short-range behavior. We observed that the bond forming and breaking processes are well described in the localized Wannier states as changes between a bonding and non-bonding orbital.<sup>8,9</sup> In metallic systems, however, situations are quite different and other practical methods should be developed.

The aim of the present work is to establish an novel extension of methodology practical in metals. We will develop a novel method based on the Krylov subspace (KS) method to achieve computational efficiency. In Section 2 we review the KS method and the density matrix is represented in the KS. An example will be presented based on our numerical results. These include a discussion of locality of off-diagonal elements of the density matrix. In Section 3, as an example of the molecular dynamics simulation, the surface reconstruction of Si(001) surface is presented. We will also show how the energy spectrum can be obtained in our developed method. In Section 4 we summarize the work presented in this paper.

## 2. Density matrix calculation based on Krylov subspace method

In this section, we will show theoretical background of the KS (Krylov subspace) method to extract density matrix for molecular dynamics simulation. Short review of the KS method is followed by analysis of its arithmetic

structure including convergence property which justifies the present method.

## 2.1 Krylov subspace method<sup>11,12</sup>

The KS (Krylov subspace) method gives the mathematical foundation of many numerical iterative algorithms such as the conjugate gradient method. This method provides an efficient way to extract the essential character of the original Hamiltonian within a limited number of basis set. Starting from a certain vector  $j_{ii}$ , a subspace of the original Hilbert space is generated by a set of vectors;

$$j_{ii}; H j_{ii}; H^2 j_{ii}; \dots; H^{K-1} j_{ii}; \quad (3)$$

The subspace spanned by the basis vectors  $\{H^n j_{ii}\}_{n=0}^{K-1}$  in eq. (3) is generally called the Krylov subspace (KS) in the mathematical textbooks. The dimension of the KS is denoted as  $K$ . We will denote the orthonormalized basis vectors in the KS as

$$|jK_1^{(i)}\rangle; |jK_2^{(i)}\rangle; |jK_3^{(i)}\rangle; \dots; |jK_K^{(i)}\rangle; \quad (4)$$

Since the matrix  $H$  is Hermitian, the Gram-Schmidt orthonormalization procedure gives one possible (but not necessary) choice of the basis set that satisfies the three-term recurrence relation called the Lanczos process;

$$b_n |jK_{n+1}^{(i)}\rangle = (H - a_n) |jK_n^{(i)}\rangle - b_{n-1} |jK_{n-1}^{(i)}\rangle; \quad (5)$$

with  $b_0 = 0$ . Hereafter we restrict ourselves to real symmetric Hamiltonian matrix,  $H$ .

From the practical point of view of calculations, the procedure of matrix-vector multiplication,  $H |jK_n^{(i)}\rangle$ , consumes the CPU time most, then the number of bases in the KS ( $K$ ) should be chosen to be much smaller than that of the original Hamiltonian matrix. This drastic reduction of the matrix size or the dimension of the KS is a great advantage for a practical large-scale calculations. The dimension of the KS  $K$  should be chosen, for example, as  $K = 30$ . We then denote the reduced Hamiltonian as  $H^K^{(i)}$  for the KS  $\{|jK_n^{(i)}\rangle\}$ .

## 2.2 Density matrix calculation in the Krylov subspace

In order to extract desired density matrix, we diagonalize the reduced Hamiltonian matrix  $H^K^{(i)}$ . Once one obtains the eigenvalue  $\epsilon^{(i)}$  and eigenvector  $|jw^{(i)}\rangle$  as

$$H^K^{(i)} |jw^{(i)}\rangle = \epsilon^{(i)} |jw^{(i)}\rangle; \quad (6)$$

the eigenvector can be expanded in terms of the basis  $|jK_n^{(i)}\rangle$ ;

$$|jw^{(i)}\rangle = \sum_{n=1}^K C_n |jK_n^{(i)}\rangle; \quad (7)$$

We introduce the density matrix operator within the KS:

$$\rho^K^{(i)} = \sum_{n=1}^K |jw^{(i)}\rangle \langle jw^{(i)}| = \frac{\epsilon^{(i)}}{k_B T}; \quad (8)$$

The essence of the present method is the replacement of the density matrix  $\rho^{(i)}$  by that of the KS  $\rho^K^{(i)}$   $|jw^{(i)}\rangle \langle jw^{(i)}|$ ;

$$\rho^{(i)} \approx \rho^K^{(i)} = \sum_{n=1}^K |jw^{(i)}\rangle \langle jw^{(i)}|; \quad (9)$$

Once this procedure is allowed, it is a great advantage from the view point of practical calculations.

Let us introduce the projection operator;

$$\hat{P}^{K(i)} = \sum_{n=1}^K |jK_n^{(i)}\rangle \langle jK_n^{(i)}|; \quad (10)$$

The crucial point is for the calculation of  $\rho^{(i)}$  that, though the state  $|j_{ii}\rangle$  is an element of the KS ( $\langle j_{ii} | j_{ii} \rangle = 1$ ), the state  $|j_{jj}\rangle$  may be not an element completely included within the KS ( $\langle j_{jj} | j_{jj} \rangle \neq 0$ ). Even so, the density matrix of the KS  $\rho^K^{(i)}$  holds the following relation;

$$\rho^{(i)} \approx \rho^K^{(i)} = \sum_{n=1}^K |jK_n^{(i)}\rangle \langle jK_n^{(i)}|; \quad (11)$$

To show eq. (11) we use a relation

$$\rho^{(i)} = \rho^K^{(i)} \hat{P}^{K(i)}; \quad (12)$$

The replacement eq. (9) is rigorous when  $K$  is equal to the dimension of the original Hilbert space. When  $K$  is much smaller, this replacement (9) can be justified only if the convergence of the summation in eq. (11) is fast enough and the contribution from large  $n$  is negligible. We will check the  $n$  dependence of both  $\rho^{(i)}$  and  $\rho^K^{(i)}$  in Subsection 2.3.

Considering the spin degeneracy, the relation of electron number  $N_{elec}$  and the chemical potential can be given as

$$\frac{N_{elec}}{2} = \sum_i \rho^{(i)} = \sum_i \rho^K^{(i)} = \sum_i \frac{\epsilon^{(i)}}{k_B T}; \quad (13)$$

which is used to determine the chemical potential in the system.

For short summary of this subsection, we note that the essential procedure is only the part reducing the dimension of the original Hamiltonian matrix  $H$  to that of the reduced matrix  $H^K^{(i)}$ . Once we obtain  $\rho^K^{(i)}$  the cost of calculating  $\rho^{(i)}$  for necessary enough number of neighboring sites and orbitals  $j$  of a fixed  $i$  is of the order of one, independent of the system size or the total number of atoms. And, furthermore, the calculation of them is perfectly parallelizable with respect to sites and orbitals  $i$ .

## 2.3 Convergence properties of the density matrix

In order to demonstrate the validity of the replacement eq. (9), we check the convergence of eq. (11). The convergence varies according to the locality of the original Hamiltonian as well as the choice of starting basis orbitals. To demonstrate the property, we choose a crystal of diamond structure with 262,144 atoms using a transferable tight-binding Hamiltonian.<sup>13</sup> We also choose the four  $sp^3$  orbitals per atom as starting basis orbitals  $\{|j_{ii}\rangle\}$ .

Figure 1 shows decay property of  $\rho^{(i)}$  ( $\rho^{(i)} = \sum_{n=1}^K |jK_n^{(i)}\rangle \langle jK_n^{(i)}|$ ) as a function of the  $n$  in the summation of eq. (11). As shown in the inset,  $\rho^{(i)}$  decays oscillatory. We plot

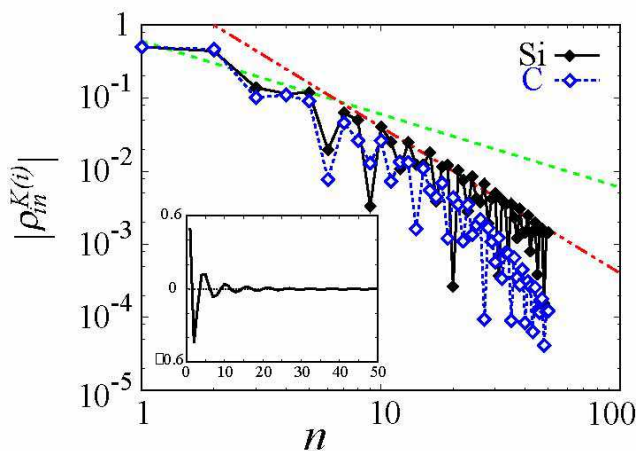


Fig. 1. Decay properties of the off-diagonal density matrix,  $\rho_{in}^{K(i)}$ , of 262,144 atom for Si (solid square with line) and that for C (open square with line). The dashed line (two dot dashed line) is a guide to the eye representing  $1/n^2$  behavior. Inset shows  $\rho_{in}^{K(i)}$  for Si in linear scale.

its absolute value to see the decay behavior. In case of silicon, we can read that  $\rho_{in}^{K(i)}$  decays as fast as  $1/n^2$ . On the other hand the value of  $\rho_{n-1,j}^{K(i)}$  depends on  $j$  but its maximum value decays as  $1/n$  (not shown in the figure) due to the fact that the state  $jK_n^{(i)}$  extends over sites reached with  $n$ -steps from the starting state  $jK_1^{(i)}$  ( $j=1$ ) to cover another localized basis  $jji$  on one site. Therefore, the products in eq. (11) decays as  $1/n^3$ . We examined several cases in different system size (512, 4096, 32768, and 262144 atoms), and found that the decay property is almost independent of the system size. In case of carbon,<sup>14</sup> on the other hand, the decay rate of  $\rho_{in}^{K(i)}$  is even more faster, which can be understood from the locality of the Wannier state.<sup>15</sup>

We note here that the choice of the starting bases as  $sp^3$  orbitals is crucial to make the dimension  $K$  of the KS smaller and the convergence faster. For diamond structure solids, the dominant interaction in the Hamiltonian is the hopping along the  $sp^3$  bond. If we ignore other hoppings in the Hamiltonian and choose a certain  $sp^3$  orbital as a starting basis, the Krylov subspace with  $k = 2$  gives the  $sp^3$  bonding and anti-bonding orbitals as

$$\frac{jK_1^{(i)} + jK_2^{(i)}}{2}; \quad (14)$$

which forms a desirable basis set in the present case. Since the choice of the starting basis is arbitrary, we can choose the four atomic orbitals,  $(s, p_x, p_y, p_z)$ , as starting basis orbitals. In such a case, however, we need sufficiently large number of steps of operating  $H$  in eq. (3) to produce  $sp^3$  orbitals on each atomic site. Therefore, the dimension of the KS could be much larger in order to obtain the similar results of the proceeding results.

We would consider an example of possible slowest convergence of eq. (11) where we can define the Fermi wave vector  $k_F$ ; Since the three-term recurrence relation in eq. (5) suggests a mapping of the original system to a one-dimensional chain model, it is instructive to com-

pare with simple consideration of one dimensional system with constant energy  $a$  and hopping  $b$  in eq. (5). This case corresponds to the one-dimensional free space, in the continuum limit, and the density matrix is given by analytic form

$$\rho_{ij}(x; x^0) = \int_{k_F}^{k_F} e^{ik(x-x^0)} dk = \frac{\sin k_F(x-x^0)}{x-x^0}; \quad (15)$$

This can be understood as  $1/n$  behaviour of  $\rho_{in}$  with oscillation. Even in this case  $\rho_{n-1,j}^{K(i)}$  decays as  $1/n$  and the products in eq. (11) decays as  $1/n^2$ . Though the analysis for other realistic systems like simple cubic lattice will be shown elsewhere, we should mention that there are several practical examples where  $\rho_{in}^{K(i)}$  decays as  $1/n$ .

Further, from the view point of practical calculations, the decay rate can be controlled by the temperature factor  $k_B T$ ; The higher the temperature, the faster the decay.<sup>16</sup> These facts validate the convergence of the summation in eq. (11) and justify the replacement eq. (9).

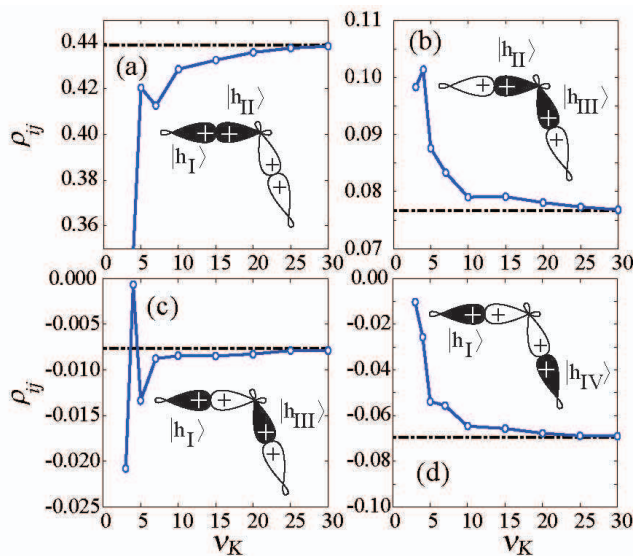


Fig. 2. Reduced matrix size dependence of the off-diagonal elements of the density matrix,  $\rho_{ij}$ , of 512 Si atoms (open circle with line). The dot dashed line represents the results of exact diagonalization of the original Hamiltonian. Inset shows schematic pictures of the  $sp^3$  hybrid orbitals  $|h_I\rangle, |h_{III}\rangle, |h_{IV}\rangle$ . Solid orbitals in each figure represent the combination to contribute the density matrix.

### 2.4 Convergence properties of off-diagonal elements of the density matrix and the total energy

As an example of the present method, we show the calculated density matrix and compare with that of diagonalization of the original Hamiltonian. We pick up two nearest neighbor bond sites along a linear path with four  $sp^3$  hybrid orbitals  $|h_I\rangle, |h_{II}\rangle, |h_{III}\rangle, |h_{IV}\rangle$ , where two orbitals  $f|h_I\rangle$  and  $|h_{III}\rangle$  and  $f|h_{III}\rangle$  and  $|h_{IV}\rangle$  are on the same bond sites and  $f|h_{II}\rangle$  and  $|h_{IV}\rangle$  are on the same atom. See inset of Fig. 2 for the configuration and the phases of respective hybrid orbitals. The

exact values of these matrix elements are calculated by the exact diagonalization of the original Hamiltonian as follows;  $\langle h_{II} | j | h_{III} \rangle = 0.439$ ,  $\langle h_{III} | j | h_{III} \rangle = 0.078$ ,  $\langle h_{II} | j | h_{III} \rangle = 0.008$ ,  $\langle h_{II} | j | h_{IV} \rangle = 0.071$ . These four are the typical elements between nearest neighbor bond sites which can be easily understood from the viewpoints of the Wannier states.<sup>10</sup>

When the dimension of the KS increases, the calculated values of off-diagonal elements of the density matrix gradually approach to the exact values and saturate. Figure 2 shows the corresponding results for Si crystal with 512 atoms. In the present case they are saturated at around  $\kappa = 30$ . The resultant convergent behavior and values are both excellent.

We note here that the convergence of the total energy could not be a unique measure of the convergence of the calculations. The convergence of the total energy is more rapid in comparison with that of the off-diagonal elements of the density matrix. In fact, the exact value of the band energy is 5.082 eV/electron and the calculated deviation from this is +80; +23; +4; +1; +0 meV/electron for  $\kappa = 7; 10; 20; 25; 30$ , respectively.

It must be mentioned that, for the present covalent bonded systems, the generalized Wannier state can be reasonably reproduced by the first order perturbation theory of the  $sp^3$  bonding orbitals and the Perturbative Order-N method is quite efficient.<sup>6,8</sup> The computational cost of the present KS method is less efficient in these systems.

## 2.5 Computational details and comparison with other methods

In actual computations, we adopt the following procedure:

- (1) Generate the Krylov subspace eq. (4) and generate eigen states within the KS by eq. (6).
- (2) Determine the chemical potential from the diagonal elements of the density matrix by using eq. (13).
- (3) Calculate the off-diagonal elements of the density matrix through eqs. (8) and (11).
- (4) Calculate forces acting on each atom and move atoms.
- (5) Return to the procedure (1).

The computational time and memory size are mostly consumed in the part of generating the Krylov subspace. The computational cost of all other procedures is actually linearly proportional to the number of atoms. Furthermore, the only global quantity we use is the chemical potential and all other calculation is purely independent with respect to each starting vector. Therefore, the computational routine is parallelizable, and actually we made use 128 and 256 parallel processors with the Message Passing Interface (MPI) technique.

Since the present method and the recursion method<sup>17,18</sup> are both based on the construction of the Krylov subspace, one might suppose that it were an extension of the recursion method. However, it is not the case. All calculations in the present method are based on the eigen values and eigen vectors in the Krylov subspace and one can calculate directly off-diagonal elements of the density matrix. On the other hands, the

recursion method is the way of calculating the diagonal Green's function in a form of the continued fraction. The discussion in the recursion method is always based on the diagonal elements of Green's functions  $G$ . The proposed way to calculate the off-diagonal Green's function in the recursion method may be<sup>17,18</sup>

$$G_{ij} = \frac{1}{2} G_{i+j;i+j} - G_{i-j;i-j}; \quad (16)$$

which needs a lot of computational resources. The recursion method would recommend, in order to calculate the off-diagonal Green's function, to use the recurrence relation of the Green's function,<sup>19</sup> but it contains potential growth of a numerical rounding error.

The density matrix actually is given by the energy integration of the Green's function in the recursion method as

$$\rho_{ij} = \frac{1}{Z} \int_{-\infty}^{\infty} d\epsilon \text{Im} G_{ij}(\epsilon) f\left(\frac{\epsilon}{k_B T}\right); \quad (17)$$

which causes a numerical error. The present method is completely free from above-mentioned difficulties in the recursion method. All calculations in the present method are based on the eigen values and eigen vectors in the Krylov subspace and one can calculate directly diagonal and off-diagonal elements of the density matrix simultaneously.

## 3. Example : results and discussions for the surface reconstruction of Si (001)

In this section, we demonstrate how the electronic structure within the KS method gives the correct atomic structure. We show the results of molecular dynamics simulation of Si (001) surface reconstruction of a slab system of 1024 atoms. The essence of the quantum mechanical freedoms is the fact that  $sp^3$ -hybrid bonds are formed in the bulk region, but not on surfaces. Specifically surface atoms move to form asymmetric dimer.<sup>20,21</sup> We will show that the asymmetry of the surface dimer is determined by the local electronic structure. We also examine total energy difference for proposed three reconstructed configurations.

### 3.1 Tilt angle of surface dimers

One of the factor to characterize the surface dimer is its tilt angle,  $\theta$ . (See inset of Fig.3 (a).) The ideal surface is energetically unstable because the surface atoms have dangling bonds. Then the surface atoms form a dimer but still a symmetric dimer,  $\theta = 0$ , is unstable. One atom moves to the bulk (lower atom) and the other moves to vacuum (upper atom) and the pair forms an asymmetric dimer. In an asymmetric dimer, the electron charge transfers from a lower atom to an upper atom and the surface energy is lowered. Theoretical and experimental data of tilt angle are reviewed in ref.<sup>22</sup> and are ranging from 5° to 19°. The reported tilt angle by the exact diagonalization of the same tight-binding Hamiltonian is 14.23°<sup>23</sup> while our result based on the KS method is  $\theta = 13.4^\circ$  with the size of the KS  $\kappa = 30$ . This result indicates that the present KS method extracts the essential character of the original Hamiltonian well. We

will discuss in the next subsection that the asymmetric surface dimer is determined by the electronic states close to the chemical potential.

### 3.2 Energy spectrum and the density of states

While methods of density matrix may usually not provide an information about energy spectrum of electronic structure, the present method can do at the same time. To discuss the electronic spectra in the framework of the KS method, we introduce the Green's function  $G_{ij}(\omega)$ ;

$$G_{ij}(\omega) = [(\omega + i\eta)H]^{-1}_{ij}; \quad (18)$$

where  $\eta$  is an infinitesimally small positive number. Since the replacement for the density matrix (9) is guaranteed, the same replacement for the Green's function is also allowed;

$$G_{ij}(\omega) \rightarrow G_{ij}^{K(i)}(\omega); \quad (19)$$

where the matrix elements of the Green's function in the KS is defined as

$$G_{in}^{K(i)}(\omega) = \frac{X^K C_i C_n}{\omega + i\eta} : \quad (20)$$

Actually the Green's function  $G_{ij}(\omega)$  can be calculated with the Green's function  $G_{in}^{K(i)}(\omega)$  in the KS as;

$$G_{ij}^{K(i)}(\omega) = \sum_n G_{in}^{K(i)}(\omega) H_{nj}^{(i)}; \quad (21)$$

The equation (21) is equivalent to (11) and can be proven similarly by using the projection operator  $\hat{P}^{K(i)}$ .

In order to single out the physical insight behind the asymmetric dimer, we calculate local density of states (DOS) per atom of the system with reconstructed surface with dimer as shown in Fig. 3(a). The DOS can be defined as

$$n_I(\omega) = \frac{1}{X} \text{Im} G_{I,I}(\omega) \quad (22)$$

$$= \sum_j \text{Im} [j \mathbf{h} \cdot \mathbf{w}^{(I)}] \rho_j(\omega); \quad (23)$$

where  $I$  and  $\mathbf{w}$  are the atomic site and orbitals, respectively, and  $\rho_j$  is sum for eigen states of the KS. First of all, we see the DOS of crystal. Because of the finite number of computed levels,  $K = 30$ , the shown DOS has thirty spikes with weight factor  $j \mathbf{h} \cdot \mathbf{w}^{(I)}$  distributed from bottom to top of the band. Here we have introduced finite imaginary part,  $\eta = 0.136\text{eV}$  ( $10^2$  Ryd), to smooth out these spiky structure. The calculated DOS of crystal reproduces the gap that lies within 0–1eV satisfactorily. The DOS of the deeper layer of the present slab system is similar to this and does not change before and after the surface reconstruction as it should be. In the DOS for dimerized surface atoms, the DOS of the upper (lower) atom has peak at 1.25 (+0.54) eV in Fig. 3(a). The former (latter) peak corresponds to occupied (unoccupied) surface state and the difference of the spectra represents the electron charge transfer from the lower atom to the upper atom

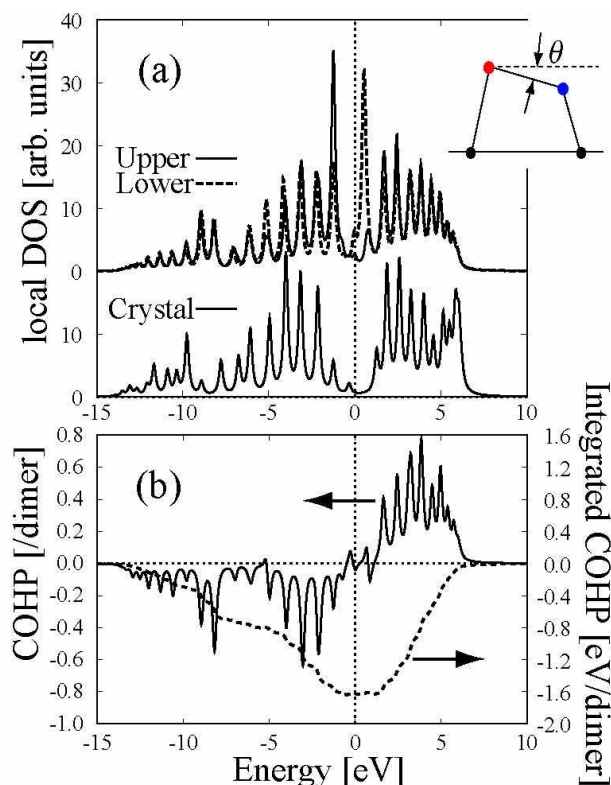


Fig. 3. (a) Local density of states (DOS) per atom for the system with asymmetric dimer and that for the system of crystal. Solid line (broken line) in upper panel represents an upper (lower) atom of the asymmetric dimer. (b) COHP and integrated COHP for the corresponding dimer. The energy zeroth both in (a) and (b) are common and is set to be the top of the occupied states in the bulk. In order to show the structure we introduce finite imaginary part,  $\eta = 0.136\text{eV}$ , in the energy denominator of the Green function. The size of the reduced matrix is  $K = 30$  and the temperature factor of the system in eq. (8) is  $T = 1580\text{K}$  ( $= 0.136\text{eV}$ ). The chemical potential is estimated as  $\mu = 0.126\text{eV}$ .

in the asymmetric dimer. In other words, this energetical separation of the occupied and unoccupied surface state is the origin of the asymmetric dimer.

We note here about the two controlling parameters to reproduce the asymmetric dimer; the size of the KS,  $K$ , and the temperature factor of the system,  $T$ . Both may affect the convergence speed in eq. (11) as well as the energy resolution of the simulation. The choice of  $K$  is important to reproduce the asymmetric dimer since the surface dimer reflects the electronic structure close to the chemical potential, in particular the occupied and unoccupied surface states. The size of the KS should be chosen so large that the profile of the surface states are well reproduced. Actually, the calculation with  $K < 20$  leads unstable value of  $\mu$ , for example,  $\mu = 0.2; 9.8; 14.5; 4.6$  for  $K = 15; 16; 17; 18$ , respectively. While those with  $K > 25$  gives stable value,  $13 \sim 14$ . We have chosen  $K = 30$ . The choice of  $T$  is also important since the surface states are energetically close to the chemical potential. The temperature should be chosen so small that the occupied and unoccupied surface states are well separated energetically. A temperature factor larger than this separation smears the structures and results in symmetric

ric dimer.

In order to see the chemical bonding in condensed matters, we introduce the following quantity;

$$C_{IJ}(\mu) = \frac{1}{X} \sum_{i,j} \text{Im} G_{I,j}(\mu) H_{j,I} \quad (24)$$

This is sometimes called the crystal orbital Hamiltonian populations (COHP).<sup>24</sup> The integration of this quantity gives cohesive energy from a pair of atoms just as the integration of local DOS gives occupation number. Actually, the total energy is decomposed into contributions of each atom pair as a sum of integration over the energy of  $C_{IJ}$ ;

$$\text{Tr}(H) = \sum_{I,j} \sum_{I',j'} H_{j,I} H_{j',I'} \quad (25)$$

$$= \sum_{I,j} \sum_{I',j'} C_{IJ}(\mu) d_{IJ} \quad (26)$$

The analysis of the COHP and the integrated COHP shows where and how the bond formation stabilizes energetically the system. The COHP for the dangling bond pair (in ideal surface) is negligible (not zero), because interaction matrix element  $H_{j,I}$  within the dangling bond pair is very small due to a larger interatomic distance. Once an surface dimer is formed (though the atomic pair is the same), the COHP gives a finite value (Fig. 3(b)), because the interatomic distance is shortened and the interaction matrix element becomes finite. The integration of the COHP has its minimum almost at the chemical potential. This is a demonstration of the cohesive mechanism of covalent bonded materials.

### 3.3 Energy difference between different configurations of dimerized Si (001) surface

The dimers may align on the Si (001) surface with three proposed reconstructed surface configurations, (2 1); (2 2); and (4 2).<sup>20,21</sup> Among them, the present calculation indicates that the (4 2) configuration is that of the lowest energy. The calculated energy differences from the (4 2) structure are 86.7 meV/dimer for  $E_{(2 1)}$  and 0.3 meV/dimer for  $E_{(2 2)}$ . These values agree well with the exact calculation using the same Hamiltonian,  $E_{(2 1)} - E_{(4 2)} = 73.6$  meV/dimer and  $E_{(2 2)} - E_{(4 2)} = 1.2$  meV/dimer, respectively.<sup>23</sup> This shows that the numerical error with the KS method is small and the present method gives a satisfactory results in a fine energy scale with tight-binding Hamiltonian. On the other hand, we should comment that the tight-binding formulation itself can be the another origin of an error. In general, the energy scale in meV/atom is too fine to discuss in the present tight-binding Hamiltonian. An *ab initio* calculation gives  $E_{(2 1)} - E_{(4 2)} = 51.21$  and  $E_{(2 2)} - E_{(4 2)} = 3.13$  meV/dimer, respectively.<sup>21</sup>

## 4. Conclusions

In the present paper we presented a novel method using the Krylov subspace for the molecular dynamics simulation based on large-scale electronic structure calculation. By means of the reliable treatment of the reduced matrix deduced from the Krylov subspace method, the

method provide an efficient and practical way to calculate the density matrix. The method also provides a way to calculate the energy spectrum on the same standpoint as the density matrix. As an example, the method is applied to the problem of the surface reconstruction of Si (001). We have pointed out through its analysis that the appropriate choice of the two controlling parameters, the size of the Krylov subspace and the temperature factor, is important. Both may affect the computational cost and the accuracy. Though the present calculation is just one example, it leads us to a general guiding principle in choosing the optimal values of the controlling parameters.

In the present methodology the computational procedure of the density matrix,  $\rho_{ij}$ , is independent for each atomic orbital,  $i$ , except the determination of the chemical potential, then the present method is very preferable for the parallel computation. Moreover, this independency of the basis lead us a hybrid scheme within quantum mechanics.<sup>8</sup> In the hybrid scheme, the density matrix is decomposed into sub matrices and the sub matrices are determined by different methods. Molecular dynamics simulation with  $10^5$  atoms by the hybrid scheme between the present KS method and the perturbative Wannier state method is examined and will be published elsewhere.

Since this newly developed method is a general theory for large matrices, the method is applicable for not only covalent bonded materials but also other systems like metal. The present KS method has a potentiality of wide applicability, even in non-Hermitian matrix, since the fundamental concept lies in the general linear algebra of large matrices.

## Acknowledgment

The authors thank S.-L. Zhang and T. Sogabe (University of Tokyo) for the discussion about the Krylov subspace method. The valuable advice about parallel computation by Yusaku Yamamoto (Nagoya University) is also grateful. Computation has been done at the Center for Promotion of Computational Science and Engineering (CCSE) of Japan Atomic Energy Research Institute (JAERI) and also partially carried out by use of the facilities of the Supercomputer Center, Institute for Solid State Physics, University of Tokyo. This work is financially supported by Grant-in-Aid from the Ministry of Education, Culture, Sports, Science and Technology and also by "Research and Development for Applying advanced Computational Science and Technology" of Japan Science and Technology Corporation.

- 1) P. Ordejon: *Comp. Mat. Sci.* 12 (1998) 157.
- 2) G. Galli: *Phys. Stat. Sol.* (b) 217 (2000) 231.
- 3) S. Y. Wu and C. S. Jayanthi: *Physics Reports* 358 (2002) 1.
- 4) W. Kohn: *Phys. Rev. Lett.* 76 (1996) 3168.
- 5) O. K. Andersen and O. Jepsen: *Phys. Rev. Lett.* 53 (1984) 2571; O. K. Andersen, T. Saha-Dasgupta, R. W. Tank, C. Arcangeli, O. Jepsen and G. Krier: in *Electronic Structure and Physical Properties of Solids*, eds. H. Dresse (Springer-Verlag, 2000) pp.3-84.
- 6) T. Hoshi and T. Fujiwara: *J. Phys. Soc. Jpn.* 69 (2000) 3773.
- 7) T. Hoshi and T. Fujiwara: *Surf. Sci.* 493 (2001) 659.

- 8) T. Hoshi and T. Fujiwara: J. Phys. Soc. Jpn. 72 (2003) 2429.
- 9) T. Hoshi: Theory and application of large-scale electronic structure calculations, Doctor thesis, University of Tokyo, 2003.
- 10) M. Geshi, T. Hoshi and T. Fujiwara: J. Phys. Soc. Jpn. 72 (2003) 2880.
- 11) G. H. Golub and C. F. Van Loan: in Matrix Computations (second edition), The Johns Hopkins University Press, Baltimore and London 1989.
- 12) Henk A. van der Vorst: in Iterative Krylov Methods for Large Linear Systems, Cambridge University Press, Cambridge, 2003.
- 13) I. Kwon, T. Biswas, C. Z. Wang, K. M. Ho, and C. M. Soukoulis: Phys. Rev. B 49 (1994) 7242.
- 14) The tight-binding Hamiltonian in the present carbon case is given by tuning the energy difference between s and p atomic orbitals ("p" "s") to be the half of that in the silicon case, according to the universal tendency of the tight-binding parameters.<sup>6,7</sup>
- 15) Our previous paper shows that the Wannier state in carbon is more localized than that in silicon as the function of bond step<sup>6,7</sup>.
- 16) The behaviour of eq.(15) originates in finite gap of the occupation number at  $k = k_F$ , known as Gibbs phenomena in applied mathematics. In finite temperature, the finite gap of occupation number vanishes, and the Gibbs phenomenon oscillations are suppressed. See, for example, G. B. Arfken and H. J. Weber: in Mathematical Methods for Physicists (Academic Press, London, 1995), Fourth edition.
- 17) R. Haydock, P. Kelly and V. Hine: J. Phys. C 5 (1972) 2845; *ibid.* 8 (1975) 2591.
- 18) R. Haydock: Solid State Phys., 35 (1980) 215.
- 19) T. Ozaki: Phys. Rev. B 59 (1999) 16061; T. Ozaki, M. Aoki and D. G. Pettifor: Phys. Rev. B 61 (2000) 7972.
- 20) D. J. Chadi: Phys. Rev. Lett. 43 (1979) 43.
- 21) A. Ramstad, G. B. Rocks, and P. J. Kelly: Phys. Rev. B 51 (1995) 14504.
- 22) J. Pollmann, P. Kugler, M. Rohlfing, M. Sabisch, and D. Vogel: Appl. Surf. Sci. 104-105 (1996) 1.
- 23) C. C. Fu, M. Weissman, and A. Saul: Surf. Sci. 494 (2001) 119.
- 24) R. Dronskowski and P. E. Blochl: J. Phys. Chem. 97 (1993) 8617.